Current-driven Magnetization Reversal in a Ferromagnetic Semiconductor (Ga,Mn)As/GaAs/(Ga,Mn)As Tunnel Junction

D. Chiba[1*], Y. Sato[1], T. Kita[2,1], F. Matsukura[1, 2], and H. Ohno[1, 2]

[1]*Laboratory for Nanoelectronics and Spintronics, Research Institute of Electrical Communication, Tohoku University, Katahira 2-1-1, Aoba-ku, Sendai 980-8577, Japan*

[2]*Semiconductor Spintronics Project, Exploratory Research for Advanced Technology, Japan Science and Technology Agency, Japan*

Abstract

Current-driven magnetization reversal in a ferromagnetic semiconductor based (Ga,Mn)As/GaAs/(Ga,Mn)As magnetic tunnel junction is demonstrated at 30 K. Magnetoresistance measurements combined with current pulse application on a rectangular 1.5×0.3 μm^2 device revealed that magnetization switching occurs at critical current densities of $1.1 - 2.2 \times 10^5$ A/cm^2. Possible mechanisms responsible for the effect are discussed.

PACS: 72.25.-b, 75.50.Pp, 85.75.-d

Corresponding author: Hideo Ohno

Laboratory for Nanoelectronics and Spintronics, Research Institute of Electrical Communication, Tohoku University, Katahira 2-1-1, Aoba-ku, Sendai 980-8577, Japan

tel/fax: +81-22-217-5553

e-mail:ohno@riec.tohoku.ac.jp

*e-mail:dchiba@riec.tohoku.ac.jp

Current-driven magnetization reversal is attracting great interest from the physics point of view as well as from the technological point of view. It may provide an alternative to the magnetization reversal using magnetic fields in magnetic memories and data storage; the reversal by magnetic fields becomes increasingly difficult when the dimension of magnetic bits is reduced, as the required field for reversal is inversely proportional to the dimension. The theoretically predicted current-driven magnetization reversal by spin-transfer torque and/or spin accumulation exerted from spin polarized currents [1, 2] has been observed mainly in magnetic metal current-perpendicular-to-the-plane (CPP) giant-magnetoresistance (GMR) structures [3-5]. The critical current required for magnetization reversal in these systems is generally high and is of the order of $\sim 10^7$ A/cm^2 or higher, which poses a difficulty to future applications. Although the general experimental features appear to be well described by the phenomenological Landau-Lifshitz-Gilbert equation with a spin-transfer-torque term, the understanding of physical processes involved in the reversal has not been fully established [6]. It is, therefore, interesting to explore whether one can observe a current-driven reversal in systems drastically different from magnetic metals. In this Letter, we present our study on current-driven magnetization reversal in magnetic tunnel junctions (MTJ) using a ferromagnetic III-V semiconductor (Ga,Mn)As [7]. (Ga,Mn)As is known to have a small magnetization of 0.1 T or less [8], high carrier (hole) spin polarization [9-11], and strong spin-orbit interaction (spin-orbit splitting at the top of valence band is 0.34 eV); the first two are expected to result in reduction of critical current, whereas the spin-orbit interaction leads to fast spin depolarization and works against reduction of critical current.

We first describe the design of our fully epitaxial (Ga,Mn)As/GaAs/(Ga,Mn)As trilayer MTJ structure. We have chosen GaAs as a barrier material, which has a barrier height of ~100 meV measured from the hole Fermi energy in (Ga,Mn)As [12]. This results in a low

resistance structure and allows us to pass a high current through it. It also exhibits high tunnel magnetoresistance (TMR) ratio, *i.e.* high carrier polarization. These (Ga,Mn)As MTJ's have shown to exhibit high TMR ratio as high as 290% at 0.4 K [11], higher than the structures employing an AlAs barrier [13]. To optimize the thickness of the GaAs barrier layer, a series of 20 nm $Ga_{0.956}Mn_{0.044}As$ / d nm GaAs / 20 nm $Ga_{0.967}Mn_{0.033}As$ MTJ's with d = 1, 2, 4, 6, and 7 nm are prepared by molecular-beam epitaxy on p^+-GaAs (001) substrate. Figure 1 shows magnetization (normalized by its saturation value M_S) versus magnetic field (M - H) curves of the samples (area ~35 mm^2). Inset shows the current-voltage (I - V) characteristics of 20×20 μm^2 devices with d = 2 and d = 6 nm at 5 K; the qualitative features of the samples having $d \le 4$ nm and $d \ge 6$ nm can be represented by the d = 2 nm and the d = 6 nm samples, respectively. A smooth M - H curve and a linear I - V curve are obtained for the d = 2 nm sample, whereas a stepped M - H curve with a nonlinear I - V curve typical of an MTJ is obtained for the d = 6 nm sample. This suggests the existence of a ferromagnetic interlayer coupling when $d \le 4$ nm. For the d = 6 nm sample, we observed over 60 % TMR at 5 K; thus d = 6 nm is thick enough to decouple the two (Ga,Mn)As layers. We, therefore, adopt d = 6 nm in the following experiments.

For the current-driven magnetization reversal experiments, an 80 nm $Ga_{0.953}Mn_{0.047}As$ / 6 nm GaAs / 15 nm $Ga_{0.953}Mn_{0.047}As$ MTJ structure on p^+-GaAs (001) substrate is prepared. Different thickness for the top and the bottom (Ga,Mn)As layers is employed in order to identify the role of the total magnetic moment of the layers. The ferromagnetic transition temperatures T_C of the top and the bottom layers are ~90 K and ~50 K, respectively, determined from the temperature dependence of M. A schematic cross-section of the completed device is shown in Fig. 2 (a). A 400 nm Cr/Au electrode is first defined by electron-beam-lithography and lift-off process, followed by mesa formation by Cl$_2$ dry-etch

using the electrode as a mask (Fig. 2 (b)). Rectangular devices having an in-plane aspect ratio of 5 are made with three different lateral dimensions of a (// [$\bar{1}$10]) × b (// [110]) = 1.5×0.3, 2.0×0.4, and 2.5×0.5 μm^2. After spinning on a 100-200 nm thick SiO_2 layer, an electrode-pad (Cr/Au) is photolithographically defined on the first Cr/Au electrode. The lead wires are bonded on the top Cr/Au pads, and the backside of the substrate through In ohmic contact.

Major and minor magnetoresistance (MR) curves of a 1.5×0.3 μm^2 device at 30 K are shown in Fig. 3 (a) measured at a bias V_d of +10 mV. Here, positive V_d (and thus current) is defined as biasing the top layer positive with respect to the bottom layer. In-plane H was applied along a (// [$\bar{1}$10]). A square TMR curve with a TMR ratio of 15% is obtained. The temperature dependence of coercive force H_C of the 1.5×0.3 μm^2 sample is shown in Fig. 3 (b), where circle and square symbols correspond to H_C determined from the TMR curves and that determined from the M - H curves of a large area (~25 mm^2) sample, respectively. The closed and open symbols show high and low H_C of the (Ga,Mn)As layers. Since T_C of the bottom (Ga,Mn)As layer is ~50 K, the layer with low H_C that vanishes at around 50 K is the bottom layer. As shown in Fig. 3 (c), H_C increases as the device dimension reduces, showing that in-plane crystalline anisotropy and/or shape anisotropy begins to take over domain wall propagation, *i.e.* the reversal process approaches the single domain limit. The origin of the different behavior of the top and the bottom (Ga,Mn)As layers is not fully understood.

In metallic CPP-GMR devices, resistance as a function of dc current is commonly used to show the current-driven effect. This approach is not suitable for the present device, because (1) the resistance under high bias voltage is two orders of magnitude higher than the metallic structures (see the inset of Fig. 4), hence heating becomes appreciable when dc current is used, and (2) the strong bias voltage dependence of TMR [11, 14] makes the

4

detection of reversal under bias difficult. Instead, we have employed the following measurement scheme: First, (1) an initial M configuration is prepared by applying external H, then (2) a 1 ms current pulse I_{pulse} of varying magnitude is applied to the device at $H = 0$, and after each pulse, (3) an MR as a function of H under a small bias $V_d = +10$ mV with H // a // $[\bar{1}10]$ is measured. Three different initial M configurations are employed, indicated as A, B, and C in Fig. 3 (a). Figure 4 shows I_{pulse} dependence of ΔR at 30 K for initial configurations A (parallel M, closed circles) and C (antiparallel M, open triangles), where ΔR is the difference between the resistance after application of I_{pulse} and the resistance with parallel M at $H = 0$. A clear switching from the initial low resistance state to a high resistance state is observed in the positive current direction for configuration A. Opposite switching is observed in the negative current direction for configuration C. Note that these low and high resistances after switching correspond to those resistances of parallel and antiparallel M configurations prepared by applying external H, respectively. In the case of configuration A (C), the initial parallel (antiparallel) M alignment switches to antipallalel (parallel) at $I_{pulse} \sim +0.8$ - $+1.0$ mA (-0.5 - -0.7 mA) or at a critical current density of $J_{AP} = (+1.9 \pm 0.3) \times 10^5$ A/cm^2 ($J_P = (-1.4 \pm 0.3) \times 10^5$ A/cm^2). These results indicate current-driven magnetization reversal in the device.

We now take a closer look at the MR curves after application of I_{pulse} greater than the threshold value. Three initial configurations (A, B, and C) are first prepared and then a current pulse is applied. Figures 5 (a) and (b) show the results on configuration A (parallel M, pointing toward the positive field direction) with $J_{pulse} = +2.2 \times 10^5$ A/cm^2. As shown in Fig. 4, application of a positive current pulse over J_{AP} results in antiparallel M and the high resistance state. When H is then applied and swept in the negative direction, the high resistance state switches to the low resistance state at -23 mT (Fig. 5 (a)), at H_C of the top layer. The direction of M of the top layer is thus unchanged after the application of the current pulse. When H is

swept in the positive direction (Fig. 5 (b)), the transition takes place at ~5 mT (H_C of the bottom layer), showing that M of the bottom layer was pointing to the negative direction after the current pulse. These two field sweeps demonstrate that the magnetization reversal takes place in the bottom layer, as M of both layers were pointing toward the positive direction under initial configuration A. Figures 5 (c) and (d) are the results of the same measurements but starting from configuration B (parallel M, pointing toward the negative direction). An opposite field dependence from that in Figs. 5 (a) and (b) is obtained. This confirms again that the magnetization reversal takes place in the bottom layer regardless of the initial direction of M. The bottom layer is thus the "free layer" that changes the magnetization direction. Because the current pulse direction in these experiments is fixed positive, we can rule out the possibility of the Oersted field generated by the pulse playing a major role in the observed reversal. The bottom layer is the free layer even when we start from the antiparallel configuration. This is shown in Figs. 5 (e) and (f), where we apply a current pulse of $J_{pulse}=$ -2.1×10^5 A/cm^2 to an antiparallel configuration C; bottom layer pointing toward the negative direction. The resulting configuration is both M pointing toward the positive direction as shown in Figs. 5 (e) and (f). Because the effect clearly depends on the current direction, heating by current pulse is not important.

Hereafter, we discuss the possible mechanisms responsible for the reversal. The effect of Oersted field and heating by current pulse can be ruled out from the experimental observation. The most probable origin responsible for the observed reversal is spin-transfer torque exerted by spin-polarized current, just like in metallic systems [1, 2]. The current direction for switching is the same direction as observed in metallic systems [3-5]. This is consistent with what we expect from the way the bands spin-split in (Ga,Mn)As; due to the negative p-d exchange interaction, electron spins aligned parallel to the Mn spins in the top

(pinned) layer are injected into the bottom (free) layer when negative I_{pulse} is applied. This exerts torque so that M of the free layer switches from antiparallel to parallel. The fact that the bottom thin layer is the free layer is consistent with the spin-transfer torque model as the total magnetic moment of the bottom layer is less than that of the thicker top layer. Under the assumption of coherent rotation of magnetization with a uniaxial anisotropy, the critical current densities for switching are calculated to be $J_P = -1.2 \times 10^6$ A/cm^2 and $J_{AP} = 3.9 \times 10^6$ A/cm^2 for our devices using the Slonczewski's formulae for CPP-GMR devices [1];

$$J_P = -\alpha e \gamma M_S d_{free}[H_A + M_S/2\mu_0]/\mu_B g(P,\pi), \tag{1}$$

$$J_{AP} = +\alpha e \gamma M_S d_{free}[H_A + M_S/2\mu_0]/\mu_B g(P,0), \tag{2}$$

where e is the elementary charge, γ the gyromagnetic ratio, d_{free} the thickness of the free layer, μ_B the Bohr magneton, and $g(P,\theta) = \left\{ -4 + (1+P)^3 (3+\cos\theta)/4P^{3/2} \right\}^{-1}$ with θ the angle of M between the top and the bottom layers. The numbers used are, 0.04 T for saturation magnetization M_S (determined at 10 K), the spin polarization $P = 0.26$ calculated from the TMR ratio of 15% using the Julliere's formula [15], and the damping constant $\alpha = 0.02$ from the reported ferromagnetic resonance data and theories [16 - 18]. The crystal anisotropy field is reported to be $2K_1/M \sim 0.1$ T and $2K_u/M \sim 0.05$ T [16, 19], where K_1 and K_u are cubic (<100>) and uniaxial ([110] or [$\bar{1}$10]) crystal anisotropy constants, respectively. Here, we employed $\mu_0 H_A = 0.1$ T as the anisotropy field; small shape anisotropy field (of the order of 0.01T) is neglected. The calculated critical current densities are an order of magnitude smaller than those in metal systems [3-5], reflecting the small magnetization of (Ga,Mn)As, but they are almost an order of magnitude greater than the observed values. Although the device size is small enough to be single domain [20], incoherent processes during reversal might be taking place, as the transition at the lower H_C (see Fig. 3) is not as sharp as the higher one, suggesting the possibility of the nucleation of magnetic domains during switching. In such a case, the domain wall propagation by the current pulse may be responsible in reducing the

threshold current density. Competition among various magnetic in-plane anisotropies (uniaxial crystal anisotropy, cubic crystal anisotropy, and shape anisotropy) [16, 19, 21] can also be a source for the non-abrupt transition, by which trapping of local M along the metastable directions may occur. Local heating could also contribute to the reduction of threshold current, as a small temperature rise results in reduction of magnetization of the bottom free layer.

In summary, we have shown that the current-driven magnetization reversal takes place in a ferromagnetic semiconductor magnetic tunnel junction. The most probable mechanism responsible for the observed magnetization reversal is the spin-transfer torque exerted from the spin polarized current. The critical current density for reversal is found to be of the order of 10^5 A/cm^2.

References

[1] J. C. Slonczewski, J. Mag. Mag. Mater. **159**, L1 (1996).

[2] L. Berger, Phys. Rev. B **54**, 9353 (1996).

[3] F. J. Albert, J. A. Katine, R. A. Buhrman, and D. C. Ralph, Appl. Phys. Lett. **77**, 3809 (2000).

[4] J. Grollier, V. Cros, A. Hamzic, J. M. George, H. Jaffrès, A. Fert, G. Faini, J. Ben Youssef, and H. Legall, Appl. Phys. Lett. **78**, 3663 (2001).

[5] F. J. Albert, N. C. Emley, E. B. Myers, D. C. Ralph, and R. A. Buhrman, Phys. Rev. Lett. **89**, 226802 (2002).

[6] Ya. B. Bazaliy, B. A. Jones, and S. C. Zhang, J. Appl. Phys. **89**, 6793 (2001).

[7] H. Ohno, Science **281**, 951 (1998).

[8] F. Matsukura, H. Ohno, and T. Dietl, in *Handbook of Magnetic Materials Vol. 14* ed. by K. H. J. Buschow, pp. 1-87 (North-Holland, 2002).

[9] T. Ogawa, M. Shirai, N. Suzuki, and I. Kitagawa, J. Mag. Mag. Mater. **196-197**, 428 (1999).

[10] T. Dietl, H. Ohno, F. Matsukura, J. Cibert, and D. Ferrand, Science **287**, 1019 (2000).

[11] D. Chiba, F. Matsukura, and H. Ohno, to be published in Physica E.

[12] Y. Ohno, I. Arata, F. Matsukura, and H. Ohno, Physica E **13**, 521 (2002).

[13] M. Tanaka and Y. Higo, Phys. Rev. Lett. **87**, 026602 (2001).

[14] J. S. Moodera, Lisa R. Kinder, Terrilyn M. Wong, and R. Meservey, Phys. Rev. Lett. **74**, 3273 (1995).

[15] M. Julliere, Phys. Lett. **54A**, 225 (1975).

[16] X. Liu, Y. Sasaki, and J. K. Furdyna, Phys. Rev. B **67**, 205204 (2003).

[17] J. Sinova, T. Jungwirth, X. Liu, Y. Sasaki, J. K. Furdyna, W. A. Atkinson, and A. H. MacDonald, Phys. Rev. B **69**, 085209 (2004).

[18] Y. Tserkovnyak, G. A. Fiete, and B. I. Halperin, cond-mat/0403224.

[19] U. Welp, V. K. Vlasko-Vlasov, X. Liu, J. K. Furdyna, and T. Wojtowicz, Phys. Rev. Lett. **90,** 167206 (2003).

[20] T. Fukumura, T. Shono, K. Inaba, T. Hasegawa, H. Koinuma, F. Matsukura, and H. Ohno, Physica E **10**, 135 (2001).

[21] K. Hamaya, R. Moriya, A. Oiwa, T. Taniyama, Y. Kitamoto, Y. Yamazaki, and H. Munekata, Jpn. J. Appl. Phys. **43**, L306 (2004).

Figure caption

Fig. 1   Normalized magnetization curves of two (Ga,Mn)As/GaAs (d nm)/(Ga,Mn)As (~35 mm^2) magnetic tunnel junction layers at 5 K (d = 2 nm and d = 6 nm). Magnetic field was applied along [$\bar{1}$10]. The inset shows I - V characteristics at 5 K of the two magnetic tunnel junction devices (20×20 μm^2) fabricated from these layers.

Fig. 2   (a) A schematic cross section of fabricated magnetic tunnel junction device structure. (b) A scanning electron micrograph of a rectangular device ($a \times b$ = 1.5 × 0.3 μm^2) after formation of the first Cr/Au electrode.

Fig. 3   (a) Major (closed symbols) and minor (open symbols) magnetoresistance curves of a 1.5×0.3 μm^2 magnetic tunnel junction sample at 30 K taken at a bias of V_d = +10 mV. Magnetic field is applied along a. (b) Temperature T dependence of coercive force $\mu_0 H_C$ and (c) size A dependence of $\mu_0 H_C$. High (low) H_C are indicated by closed (open) symbols. Squares in (b) are $\mu_0 H_C$ of the 25 mm^2 sample determined from magnetization measurements, and circles are $\mu_0 H_C$ of the 1.5×0.3 μm^2 sample determined from TMR signals.

Fig. 4 ΔR as a function of I_{pulse} of the 1.5 × 0.3 μm^2 device at 30 K, where ΔR is the resistance difference between the resistance of MTJ after application of I_{pulse} (1 ms) and that at parallel magnetization configuration at H = 0. Closed circles show the I_{pulse} dependence of ΔR for initial configuration A (parallel M), whereas open triangles show the results for initial configuration C (antiparallel M). The inset shows I-V characteristics of the device.

Fig. 5 Magnetoresistance curves of the 1.5×0.3 μm^2 device at 30 K measured at V_d = +10 mV starting from three different states. MR curves (a) and (b) are obtained from a state prepared by applying a positive current pulse with current density of J_{pulse} = + 2.2 × 10^5 A/cm^2 on initial configuration A (see the rightmost diagram for M configuration). MR curves (c) and (d) are obtained from a state prepared by the same manner but starting from initial configuration B. Curves (e) and (f) are from a state prepared by applying a negative current pulse with current density of J_{pulse}= -2.1×10^5 A/cm^2 on initial configuration C.

Fig.1. Chiba *et al.*

(a)

Cr/Au

(Ga,Mn)As

SiO$_2$

GaAs

p$^+$-GaAs sub.

(Ga,Mn)As

(b)

[$\bar{1}$10]

[110]

1 μm

Fig.2. Chiba *et al.*

30 K, V_d = +10 mV — (a) — R (kΩ) — MR (%) — C — B — A — 1.5 x 0.3 μm^2

$\mu_0 H$ (mT)

$\mu_0 H_C$ (mT) — (b) — 25 mm^2 — 1.5 x 0.3 μm^2 — T (K)

(c) — 1.5 x 0.3 — 2.0 x 0.4 — 2.5 x 0.5 μm^2 — 30 K — A (μm^2)

Fig.3. Chiba *et al.*

15
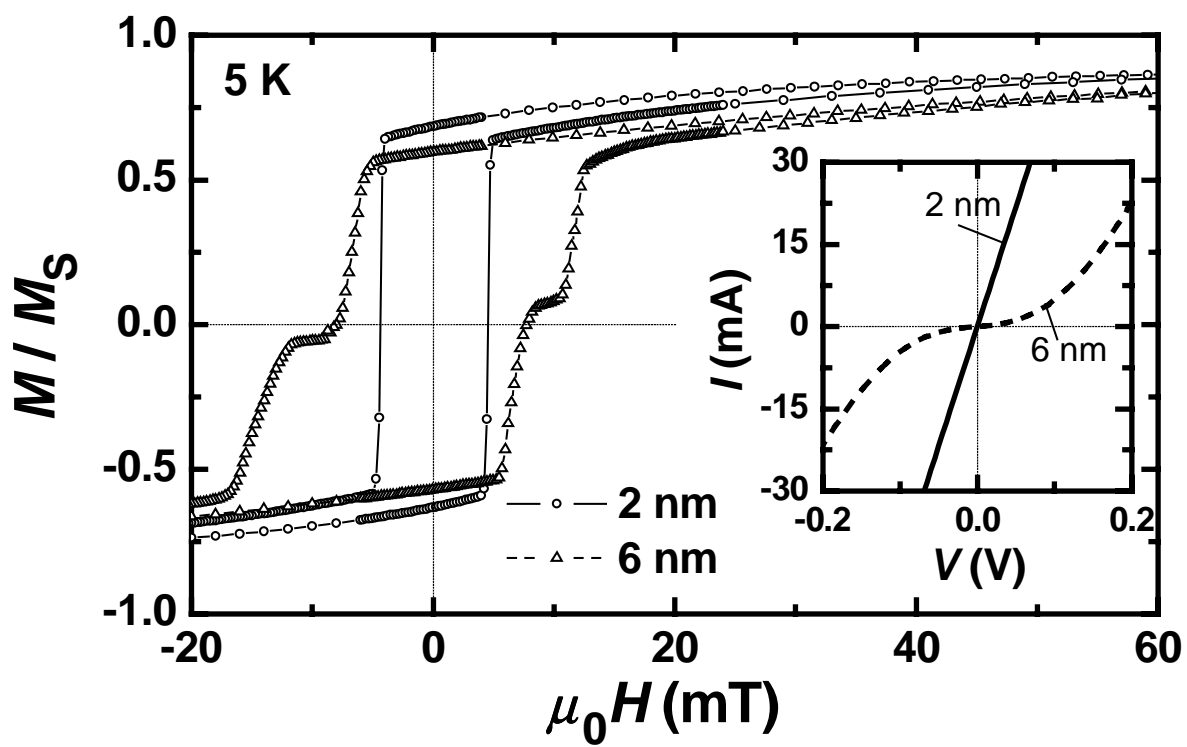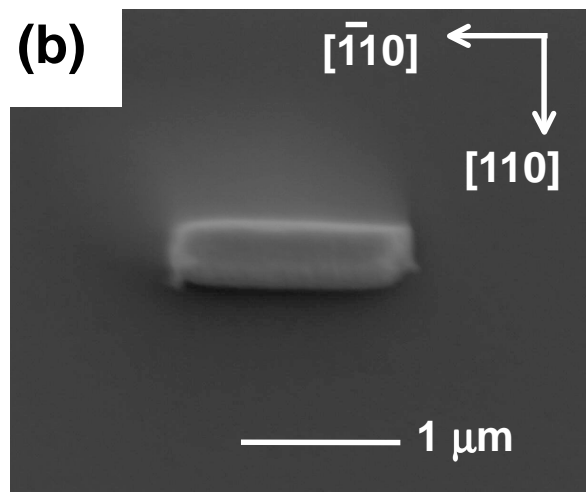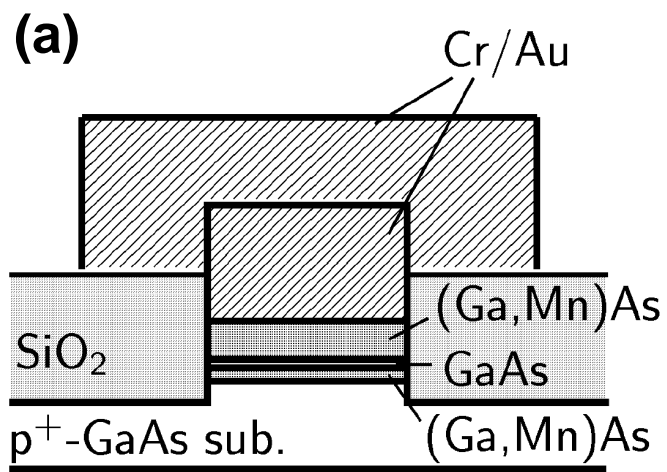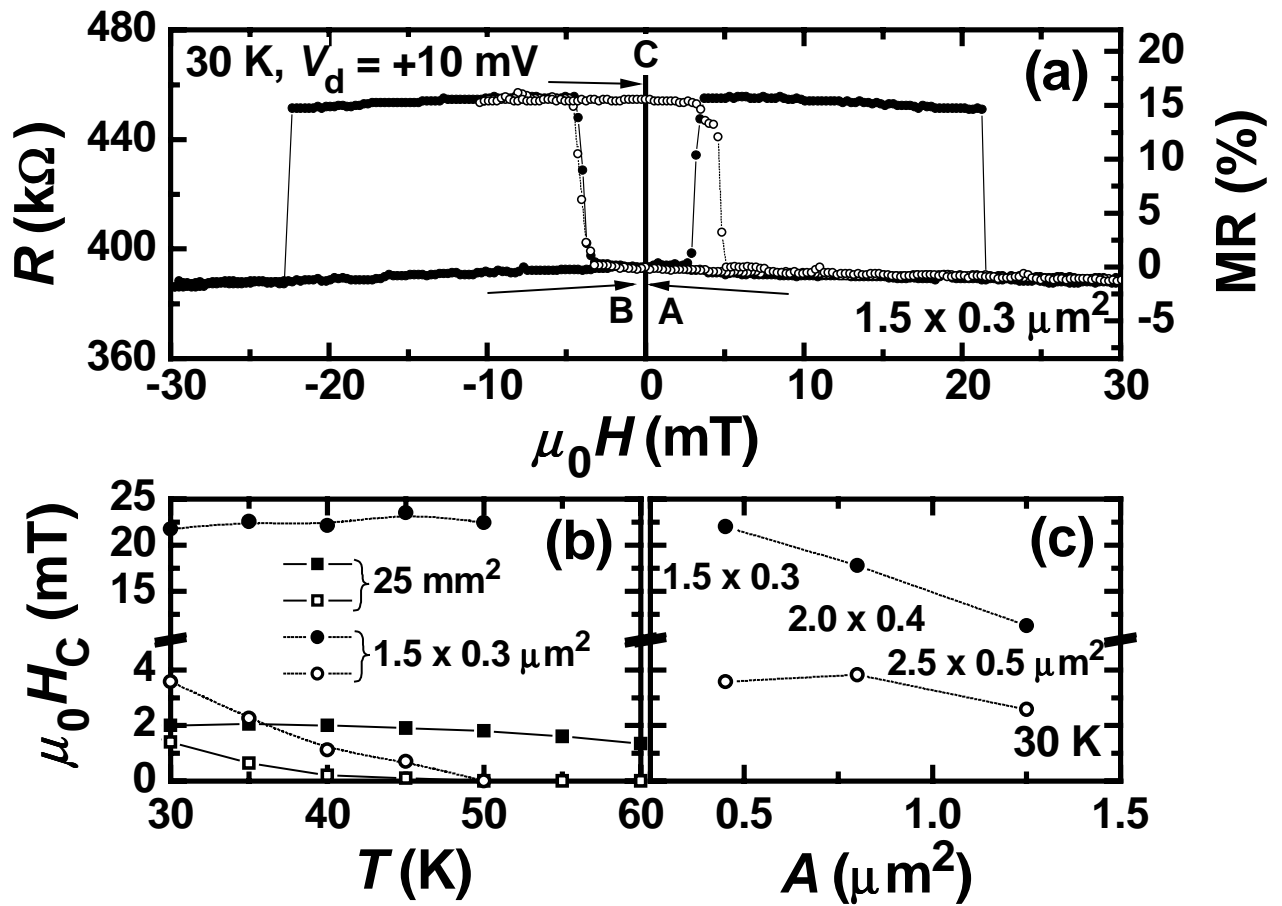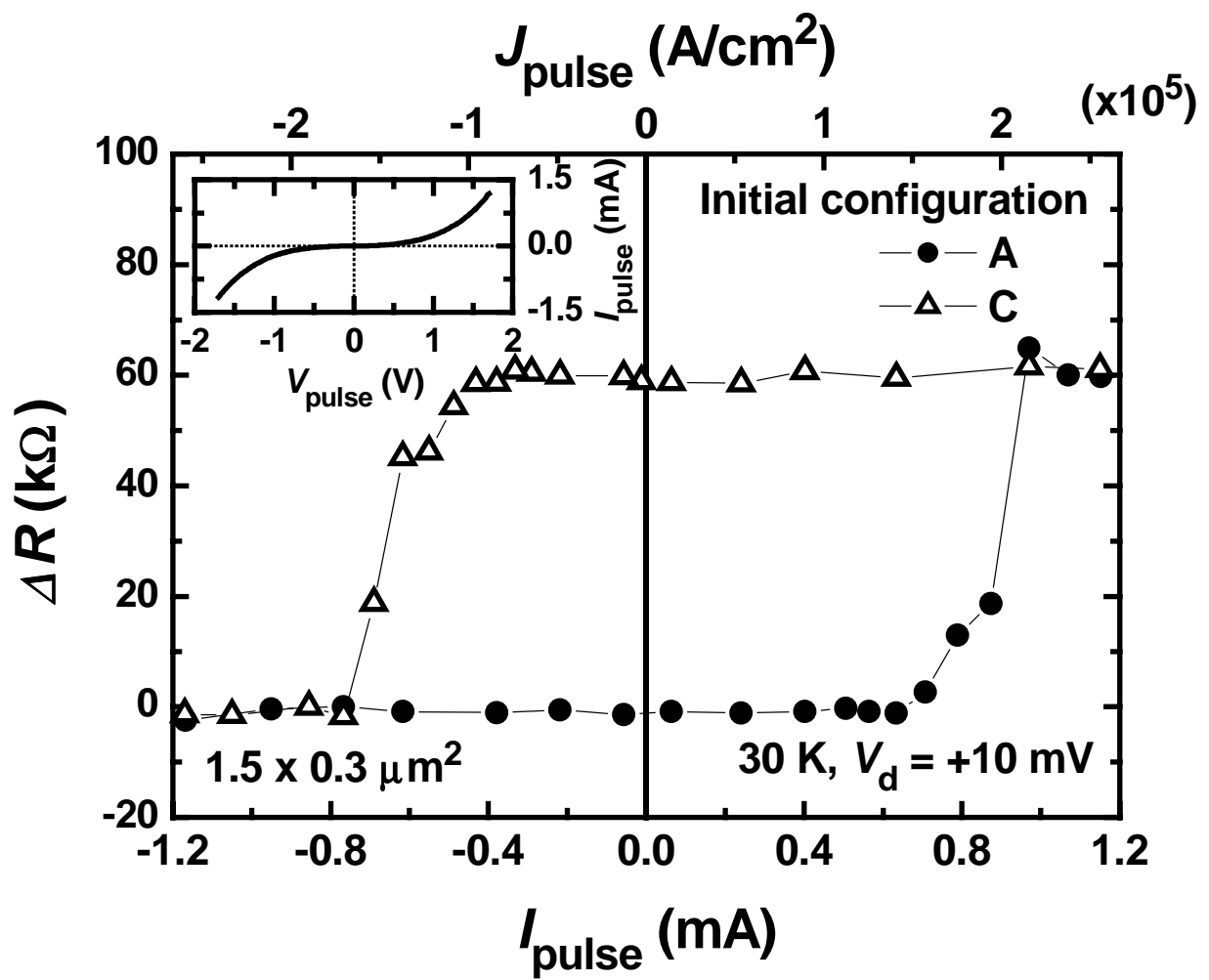
Fig.4. Chiba *et al.*

Fig.5. Chiba *et al.*